Precision Engineering 74 (2022) 186–194

Contents lists available at ScienceDirect

Precision Engineering

journal homepage: www.elsevier.com/locate/precision

Flexible fabrication of Fresnel micro-lens array by off-spindle-axis diamond turning and precision glass molding

Lin Zhang [a], Allen Y. Yi [b], Jiwang Yan [a,*]

[a] Department of Mechanical Engineering, Faculty of Science and Technology, Keio University, Yokohama, 223-8522, Japan
[b] Department of Integrated Systems Engineering, The Ohio State University, 210 Baker Systems Engineering Building, 1971 Neil Ave., Columbus, OH, 43210, USA

ARTICLE INFO

Keywords:
Fresnel micro-lens array
Off-spindle-axis diamond turning
Precision glass molding
Optical components
Structured surface

ABSTRACT

Fresnel micro-lens arrays with close-to-wavelength features have significant advantages in minimization of optical systems. However, in the fabrication of a Fresnel micro-lens array by conventional diamond turning, the discontinuous features of the surface profile cause interference between the tool flank face and the finished surface. In this manuscript, a novel off-spindle-axis diamond turning method is proposed to fabricate Fresnel micro-lens array mold insert and a toolpath generation algorithm is developed. The generation of each lenslet is treated as an independent turning operation, and the whole fabrication of a Fresnel micro-lens array is completed by a succession of repetitive turning operations. With this approach, the interference between the tool and the finished surface is avoided, and the form accuracy and surface integrity are improved for each lenslet. Then, the Fresnel micro-lens array mold insert is further utilized in precision glass molding to replicate the micro-lens structures onto transparent polymer substrates. The experimental results indicate that both the diamond-turned and molded Fresnel micro-lens arrays are achieved with homogeneous quality. As an application, a compact imaging system based on the molded Fresnel micro-lens array is demonstrated. The proposed machining method in this study can be employed in the fabrication of Fresnel micro-lens arrays and other micro-optics with discontinuous profiles with high accuracy and machining efficiency.

1. Introduction

Fresnel lens is a type of composite compact lens, which fulfills the requirements on large aperture and short focal length, but less material required by a lens of conventional design. It is particularly employed in lighthouses and searchlights to concentrate the light into a relatively narrow beam, while it also gains wide applications in cameras, solar cells, sensors and photonic devices [1–3], since it can be made much more compact than a comparable conventional lens. Originally, the Fresnel lens was generally designed and used as one independent unit with large aperture. Recently, the minimization of both imaging and non-imaging systems clearly demonstrates the need for a more compact, flexible, and cost-effective alternative [4,5]. Instead, the micro-optics array consists of a large number of lenslets with intricate surface profiles have received more and more attention due to their inconceivable capabilities providing optical engineers with great freedom to optimize imaging performance, integrate multiple functions and minimize the dimension of optical systems. These micro-optics are generally inherent with complex freeform profiles and discontinuous structures. The requirement for surface integrity and form accuracy are comparable or even higher than that for some conventional lenses. Thus, the intricate profiles of micro-optics impose great challenges to the current fabrication approaches, including single-point diamond turning and precision glass molding, for cost-effective fabrication of micro-optics arrays with high form accuracy and good surface integrity.

In order to satisfy the demands of various micro-optics arrays, numerous fabrication techniques have been proposed. According to material removal mechanism, these approaches can be classified into chemical [6–8], physical [9,10] and mechanical machining [11–13]. Nevertheless, for the majority of these physical and chemical methods, the surface geometries and applicable materials are restricted to a few choices. In addition, it is usually difficult to obtain the finished profiles with well-defined intricate shapes or homogeneous surface integrity [14]. Compared with the abovementioned methods, mechanical machining is more universal and deterministic in intricate surface fabrication on a wide range of engineering materials, involving metallic alloys, polymeric composites and so on. Two typical mechanical approaches, high-speed diamond micro-milling and single-point diamond

* Corresponding author.
E-mail address: yan@mech.keio.ac.jp (J. Yan).

https://doi.org/10.1016/j.precisioneng.2021.11.013
Received 27 June 2021; Received in revised form 24 September 2021; Accepted 17 November 2021
Available online 18 November 2021

turning, are widely implemented in optical fabrication. For high-speed diamond micro-milling, a ball milling tool is mounted on a high-speed spindle. Each lenslet is treated as an individual unit and the whole micro-lens array can be fabricated one by one with repetitive operations, which is a feasible method of obtaining uniform quality for all lenslets [12,15,16]. However, limited by the size of the diamond milling tool, it is hard to satisfy the increasing demands for the micro-optics with micro/nano discontinuous features [17].

Single-point diamond turning machining process has superiority on ultra-high form accuracy and wide choices on engineering materials, which has been widely accepted as one of the most popular methods in optical fabrication [13,18,19]. Many researches on micro-optical fabrication are based on F/STS diamond turning [4,11,13,18–20]. Nevertheless, some inevitable discontinuous profiles of micro-optics may lead to tool irregular vibration, deteriorate surface integrity, and induce form error. Furthermore, some special features of diffractive micro-optics cause severe interference between the tool flank face and the finished surface. Therefore, a novel toolpath generation strategy should be introduced to overcome these issues and realize more flexible F/STS diamond turning for fabrication of intricate micro-optics array with discontinuous features.

With respect to some specific discontinuous features, several F/STS diamond turning methods have been proposed. For example, diamond micro-chiseling (DMC) was proposed by Brinksmeier et al. to fabricate the retro-reflective array [4], and the special guilloche machining technique (GMT) was induced to generate polygonal Fresnel lens array [21]. However, both of these aforementioned methods are only suitable for some specified discontinuous features without flexibility to generate variable structures [22]. Recently, the concept of virtual spindle tool servo proposed by To et al. [23], introduces a possible way to fabricate Fresnel micro-optics array with discontinuous features in large area by F/STS diamond turning.

Although single-point diamond turning provides an appropriate method in optical fabrication, it is not suitable for mass production of optical elements [17]. Precision glass molding (PGM) is a near net-shape replication process, which is suitable for large-volume replication of optical elements due to its high efficiency, short cycle time and reusable tool [24]. In a typical PGM process, a glass preform is located between the upper and lower mold inserts, which is further driven into the mold cavity and conformed to the desired shape at the molding temperature. The molded optics can be applied in various optical systems without further treatment. The precision glass molding provides the photonics industry an excellent mass fabrication process for low-cost and high-accuracy optical elements [25].

In this manuscript, to achieve flexible fabrication of Fresnel micro-lens array, the strategy of virtual spindle tool servo and spiral toolpath are combined in mold insert fabrication. The virtual spindle tool servo enables flexible shifting the virtual spindle to coincide with the axis of each lenslet, and the Fresnel structure is generated by a spiral toolpath generated in the local coordinate system. The principle and spiral toolpath generation algorithm of the proposed technique are provided in detail. To validate the feasibility and evaluate the machining efficiency of the proposed method, a 3 × 3 Fresnel micro-lens array is test-fabricated on a metallic mold insert. Then, the diamond turned Fresnel micro-lens array mold insert is employed in precision glass molding to replicate the optical features to polymer substrates. Both the form accuracy and surface roughness of the diamond-turned and the replicated sample are evaluated. Furthermore, the molded Fresnel micro-lens array is assembled into a compact imaging system to determine the optical performance and the fidelity of the optical elements.

2. Principle on generation of fresnel micro-lens array

To avoid the interference between the tool flank face and the finished surface, the clearance angle of the diamond tool should be larger than the slope of the desired profiles along the cutting direction.

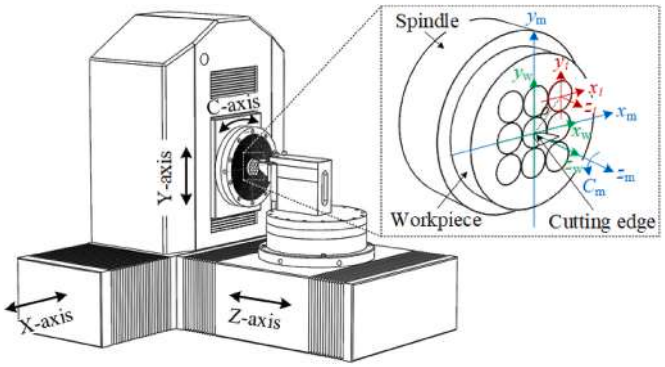

Fig. 1. Schematic diagram of hardware configuration of off-spindle-axis diamond turning.

Nevertheless, large clearance angle will aggravate the tool wear and remarkably reduce the stiffness of the diamond tip. For discontinuous surface profile, Fresnel micro-lens as an example, the surface profile can be fabricated only when the main spindle axis coincides with its axial-symmetry axis. If not, collisions between the diamond tool and the finished surface interrupt the turning operation. The conventional diamond turning method appears to be quite helpless in such discontinuous profile fabrication even increasing the clearance angle.

Facing this issue, an alternative machining method is proposed by combining the advantages of the virtual spindle tool servo with spiral toolpath generation. Each lenslet, as an independent cell, is separately fabricated using an independent spiral toolpath by shifting the virtual spindle to the center of each cell. The whole process consists of a succession of repetitive diamond turning operations. So only the determination of the toolpath for one single lenslet is required and the whole fabrication is completed by shifting the virtual spindle to pass through all the centers of lenslets in sequence. The kinematics and toolpath generation algorithm are proposed.

2.1. Kinematics of off-spindle-axis diamond turning

In order to achieve off-spindle-axis diamond turning, three linear motions and a rotatory motion should be synchronized to generate a spiral toolpath around the virtual spindle. As shown in Fig. 1, the CNC lathe consists of three linear motions along X-, Y- and Z-axis slides, and a rotatory motion around C-axis. The specimen is mounted on a jig and then attached to the vacuum chuck. The diamond tool is fixed on the tool turret. The global coordinate system of the machine system o_m-$x_m y_m z_m$ is fixed on the main spindle, where z_m-axis is coincident with the work spindle axis, x_m- and y_m-axis are parallel with the X- and Y-axis slides. At the initial stage, the workpiece coordinate system o_w-$x_w y_w z_w$ is coincided with the global coordinate system o_m-$x_m y_m z_m$. The original point O_i of local coordinate system o_i-$x_i y_i z_i$ is located at the center of the ith lenslet, and the x_i-, y_i- and z_i-axis share the same directions with the x_m-, y_m- and z_m-axis in global coordinate system.

As shown in Fig. 2(a), one lenslet cell is located at a distance of ρ with the initial angle θ between $O_m O_i$ and x_m-axis ($t = 0$). When the vacuum chuck rotates around C-axis with a constant angular velocity ω during a period of t, the position of the lenslet is changed from its initial position. The new position after duration of t for the lenslet cell is shown in Fig. 2 (b). It is clearly noted that the motion of the center point O_i in this process can be decomposed into two harmonic oscillations along x_m- and y_m-axis, with the same amplitude of ρ but $\pi/2$ phase difference. In addition, the local coordinate system o_i-$x_i y_i z_i$ also rotates around its axis with the same angle, which means these two coordinate systems share the same characteristics on angular motion. Based on the motion analysis, the diamond tool can follow the motion of the local coordinate system by composing x_m- and y_m-axis motions. The spiral diamond toolpath for each cell is shown in Fig. 2(c). By the same way, the local

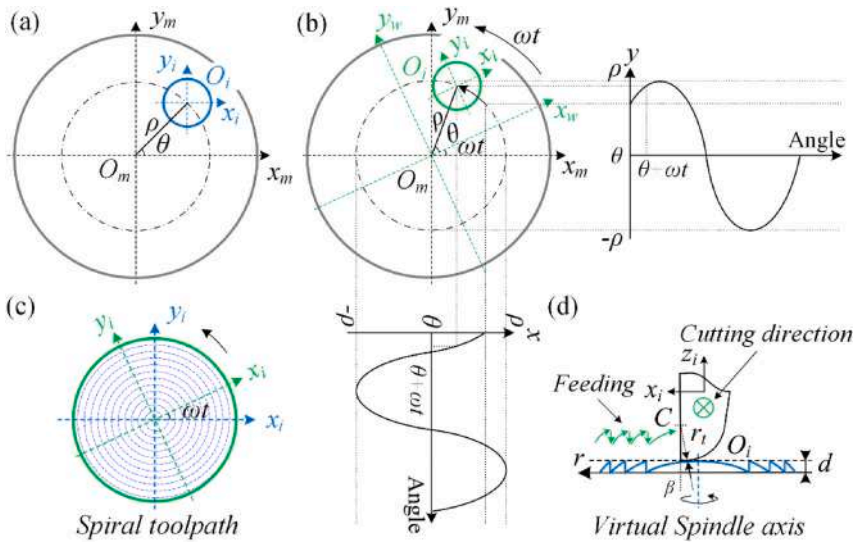

Fig. 2. Schematic diagrams of the basic principle for off-spindle-axis diamond turning, (a) initial status, (b) C-axis spindle rotation with an angle of ωt, and in local coordinate system (c) spiral toolpath for diamond turning and (d) diamond tool motion on 2D cross-section profile.

spiral toolpath can be further implemented with the angular velocity ω. Based on the analysis on 2D cross-section profile shown in Fig. 2(d), each Fresnel lenslet can be fabricated by spiral toolpath in local coordination system without difficulties or interferences stated above.

2.2. Toolpath generation strategy

As stated above, the whole fabrication process consists of a succession of repetitive turning operations. Only one spiral toolpath for an arbitrary lenslet should be determined and the toolpaths for other lenslets can be derived and obtained based on the relative positions between them [26].

As shown in Fig. 2(a), the original point O_i of the local coordinate system o_i-$x_iy_iz_i$ in the global coordinate system o_m-$x_my_mz_m$ can be expressed as follows,

$$\begin{cases} x_m = \rho\cos(\theta+\omega t) \\ y_m = \rho\sin(\theta+\omega t) \\ z_m = 0 \end{cases} \tag{1}$$

where θ is the initial angle between the O_mO_i and x_m-axis. ωt is the rotation angle after the duration of t. ρ is the distance between the original points of global coordinate system and local coordinate system (O_m-O_i).

For the local spiral toolpath, f is set as the feed per revolution along x_i-axis. The position of the jth tool contact point can be expressed in the local coordinate system o_i-$x_iy_iz_i$ as follows,

$$\begin{cases} x_i^j = \dfrac{f}{2\pi}\omega t \\ y_i^j = 0 \\ z_i^j = D(x_i^j, y_i^j) \end{cases} \tag{2}$$

where $D(x_i, y_i)$ defines the surface profile of each lenslet.

To compensate the tool nose radius, as shown in Fig. 2(c), the center of tool nose radius (point C) has the following relationship with the jth tool contact point in the local coordinate system o_i-$x_iy_iz_i$ as follows,

$$\begin{cases} x_i^C = x_i^j + r_t\sin\beta \\ y_i^C = 0 \\ z_i^C = z_i^j + r_t\cos\beta \end{cases} \tag{3}$$

where r_t is the tool nose radius. β is the angle between the unit normal vector of the surface profile at the jth tool contact point and the z_i-axis.

The position of point C in the global coordinate system o_m-$x_my_mz_m$ can be obtained based on the principle of motion composition, which can be further determined as follows,

$$\begin{cases} x_m^C = x_m + x_i^C = \rho\cos(\theta+\omega t) + \dfrac{f}{2\pi}\omega t + r_t\sin\beta \\ y_m^C = y_m + y_i^C = \rho\sin(\theta+\omega t) \\ z_m^C = z_m + z_i^C = z_i^j r_t\cos\beta \end{cases} \tag{4}$$

By repeating the aforementioned calculations throughout all the

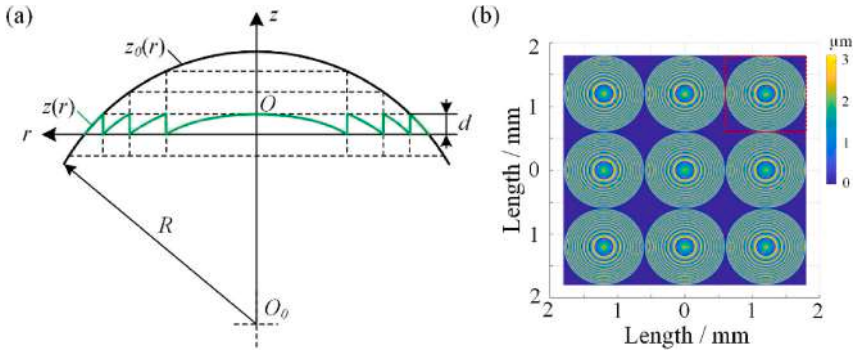

Fig. 3. Schematic diagrams of (a) the surface profile of a Fresnel lens and (b) the model for the 3 × 3 Fresnel micro-lens array.

Table 1
Parameters for the Fresnel micro-lens array.

Parameters	Values
Dimension/mm^2	3.6 × 3.6
Aperture/mm	1.20
Curvature/mm	3.91
Zone depth/μm	3.164
Conic constant	2.2165

lenslets, a succession of toolpaths for the Fresnel micro-lens array can be determined. In the turning operation, the linear motions in global coordinate system, x_m-, y_m- and z_m-axis, are achieved by the movement of X-, Y- and Z-axis slides of the machine tool, while the main spindle *C*-axis provides a constant rotation speed.

2.3. Surface profile

Fig. 3(a) shows the surface profile of the Fresnel lens. The profile of the Fresnel lens can be simplified from that of the aspherical surface. The surface profile of an aspherical lens $z(x)$ is generally expressed in Zernike polynomials as follows,

$$z(x) = \frac{Cx^2}{1+\sqrt{1-(k+1)C^2x^2}} + \sum_{i=1}^{m} a_i x^i \tag{5}$$

Here $C = 1/r$, where r is the radius of curvature. x is the distance from the optical axis z and k is the conic constant. N is the number of polynomial coefficients and a_i is the coefficient for the ith extended polynomial term. For the aspherical surface, the $a_i = 0$ and $k = -n^2$ are adopted in the optical design. The surface profile can be described as the following equation,

$$z(x) = \frac{Cx^2}{1+\sqrt{1-(1-n^2)C^2x^2}} \tag{6}$$

Then, the aspherical lens surface is cut into a succession of concentric rings by cylindrical surfaces with a constant step. The radial coordinate of each zone step can be calculated as following [27],

$$x_j = \sqrt{j \cdot d\left(\frac{2}{C} - j \cdot d\right)} \tag{7}$$

where j is the sequential number of the Fresnel zone counted from the optical axis z, and d is the zone depth. Detailed parameters for the Fresnel micro-lens array are listed in Table 1 and the designed 3 × 3 Fresnel micro-lens array is shown in Fig. 3(b). For the mold insert, the surface profile should be the inverse of the designed optical profile. The marked lenslet in Fig. 3(b) is further extracted for the analysis on spiral toolpath generation in the following section.

In order to provide an intuitionistic description of the toolpath and kinematic characteristics, the toolpath for the Fresnel micro-lens array is generated by Matlab program following the toolpath determination strategy proposed above. The toolpath for the lenslet marked in Fig. 3(b) is presented in global coordinate system and local coordinate system, as illustrated in Fig. 4(a) and (b), respectively. The feedrate is set as 20 μm/rev to have a clear view of the toolpath. In the global coordinate system, unlike the spiral toolpath in conventional diamond turning, the toolpath no long rotates around the main spindle axis as a spiral trajectory. The generated toolpath is much clear in the local coordinate system shown in Fig. 4(b). It can be seen that the toolpath is a set of independent spiral trajectories with a constant interval around the local coordinate system z_i-axis. As the analysis of the motions illustrated in Fig. 4(c), the motions in x_m- and y_m-axis oscillate at the same frequency with $\pi/2$ phase difference, while the motion in z_m-axis follows the surface profile of the lenslet. The frequency of the oscillation is exactly the same with that of the main spindle rotation. In addition, the kinematic characteristics of the diamond tool, including the position and velocity, are also obtained, as shown in Fig. 4(d). A smooth tool path for each lenslet is achieved except a few interruptions, verifying the feasibility of the proposed toolpath generation strategy above. The interruptions of the z_m-axis

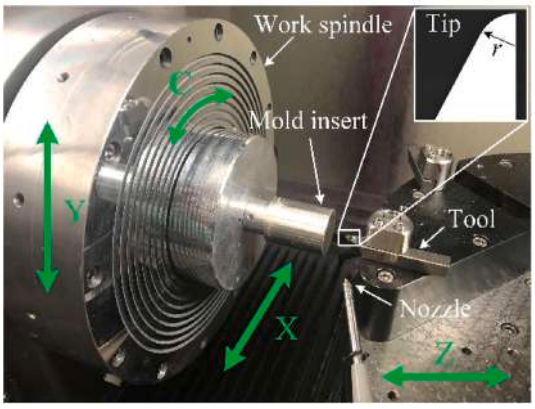

Fig. 5. View of the diamond turning experiment for Fresnel micro-lens array mold insert.

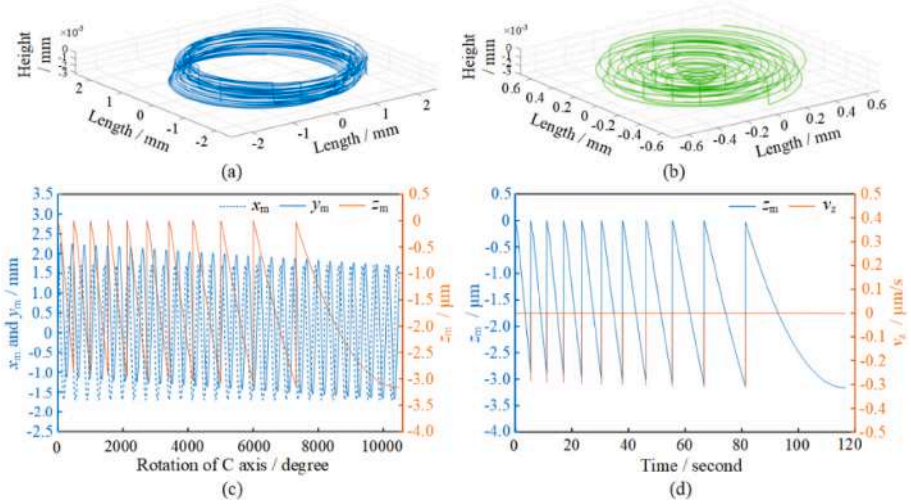

Fig. 4. The toolpath of the selected lenslet in off-spindle-axis diamond turning in (a) global coordinate system, and (b) local coordinate system, and the corresponding kinematic characteristics of (c) the x_m-, y_m-, and z_m-component of the proposed toolpath, and (d) the position and velocity of the z_m-component.

Table 2
Turning parameters for Fresnel micro-lens array mold insert.

Parameters	Values
Material	6061 Aluminum alloy
Diamond tool	Half-round edge tool
Tool radius r/mm	0.045
Rake angle/°	0
Clearance angle/°	8
Rotation speed/rpm	15
Cutting speed/mm/min	0–56.5
Spiral pitch f/μm	5.0
Depth of cut/μm	0–3.164
Coolant	Spray mist

motion should be attributed to the discontinuous profile of the Fresnel micro-lens.

3. Experimental setup

3.1. Off-spindle-axis diamond turning

The diamond turning experiments are performed on a five-axis ultra-precision machine tool (Moore 350FG, Moore Nanotechnology Inc., USA) to verify the proposed off-spindle-axis diamond turning for Fresnel micro-lens array, as shown in Fig. 5. The C-axis spindle can maintain angular position to less than 1 arcsec and linear axes are with positioning resolution of 0.1 nm. The mold material is 6061 Aluminum alloy and a commercial natural diamond tool with tool nose radius of 0.045 mm (Contour Fine Tooling, UK) is adopted in diamond turning. The rake and clearance angles are 0° and 8°, respectively. Before diamond turning, the mold insert is rough-machined on a CNC 3-axis vertical milling machine (Haas VF-3, Haas Automation, Inc., USA) from a 6061 Aluminum alloy rod. After the mold insert is clamped on the vacuum chuck, the mold insert surface is firstly flattened by diamond facing to achieve a smooth surface. Then, the Fresnel micro-lens array is engraved on the smooth surface. The cutting speed is varying with workpiece radius from 0 to 56.5 mm/min, which might have some slight influence on the surface quality. However, since the diamond turning is performed under a slow tool servo mode, the cutting speed is kept slow and the effect of its variation is negligibly minor. To fabricate the Fresnel micro-lens array, the diamond tool periodically contacts and departs from the specimen with a smooth toolpath except a few inevitable interruptions due to the discontinuous features on the surface profile. Finally, the finished surface is cleaned by acetone and alcohol to remove the residual coolant and attached chips on the finished surface. The detailed conditions of diamond turning experiment are summarized in Table 2.

3.2. Precision glass molding

The precision glass molding is conducted by a commercial precision glass molding machine (GMP-211, Toshiba Inc., JP). The molding material used in the experiment is Poly(methyl methacrylate) (PMMA). The glass transition temperature (T_g) of PMMA is 105 °C. The preform is a double-side polished circular plate with 25.4 mm diameter and 2.0 mm thickness. Fig. 6(a) illustrates the precision glass molding process, which can be divided into three stages: (1) heating, (2) pressing and (3) cooling. At the initial stage, the preform is placed between the upper and

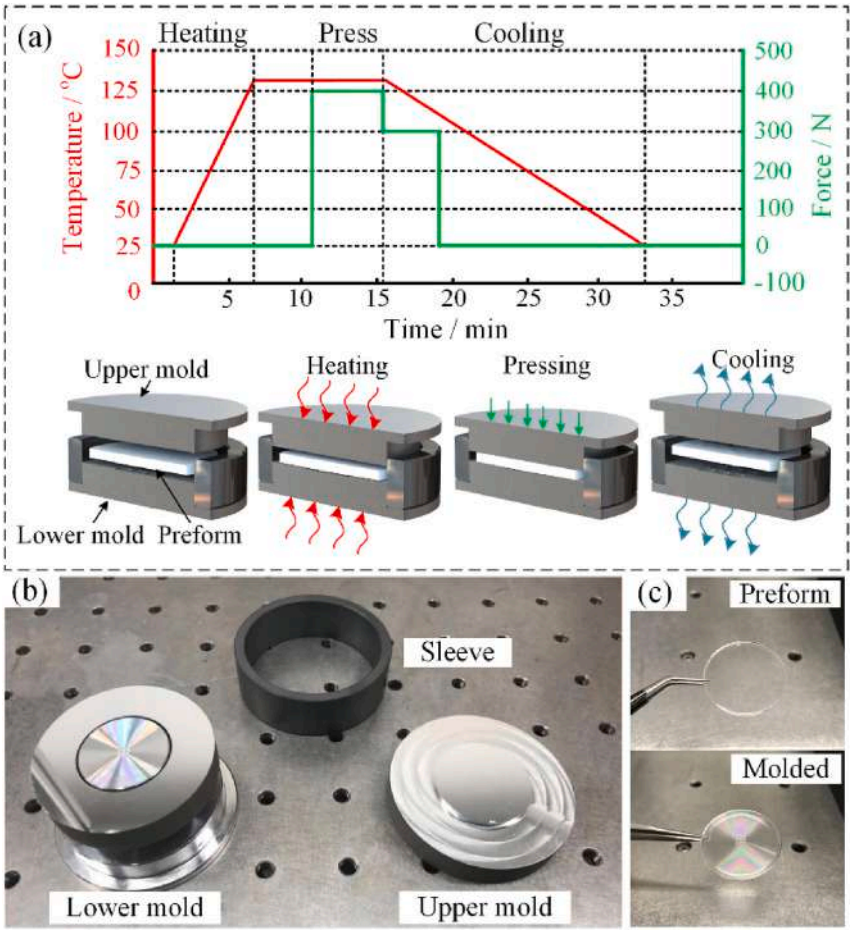

Fig. 6. Schematic diagrams of (a) precision glass molding process, and photographs of the (b) Fresnel micro-lens array mold assemblies, and (c) preform and molded Fresnel micro-lens array.

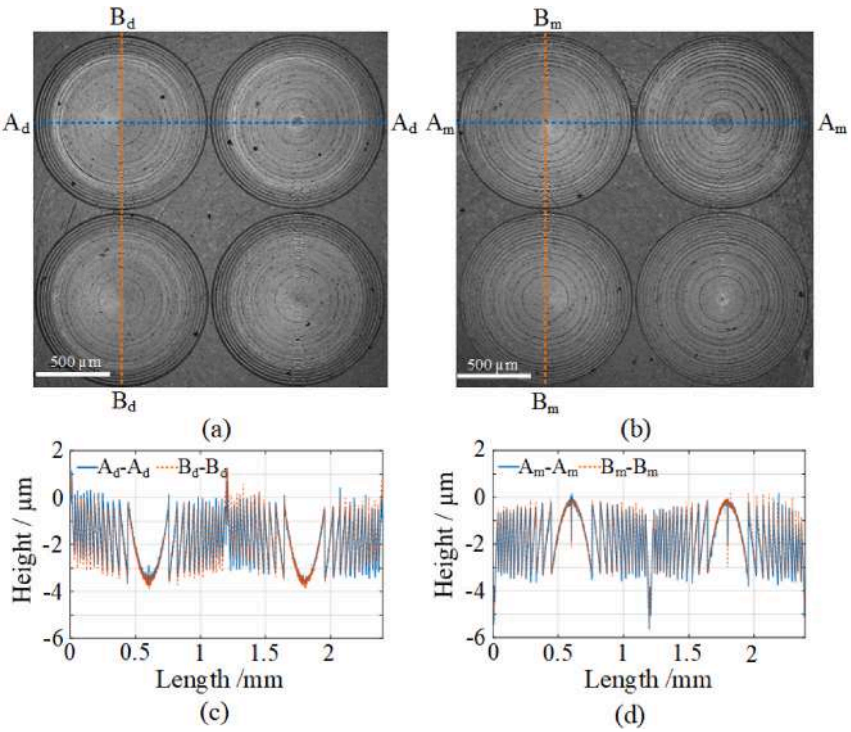

Fig. 7. Optical images of the Fresnel micro-lens array on the (a) diamond turned mold insert and (b) molded Fresnel micro-lens array with magnification of 5×, and 2D profiles along the cross-hair directions on the (c) diamond turned mold insert and (d) molded Fresnel micro-lens array.

lower molds, and the chamber is purged with argon gas to get rid of oxygen. Then, the preform and mold assemblies, as shown in Fig. 6(b), are heated up to the molding temperature 135 °C with protective gas shield. After maintaining the temperature for ~5 min, the lower mold moves upwards to press the preform with the velocity of 0.2 mm/s. To ensure the cavity is completely filled, the preform is continuously pressed with the maximum load of 400 N until the position of lower mold remains unchanged for ~5 min. Then, a cooling stage with 0.1 °C/s until 25 °C is followed after the pressing stage. To improve the replication accuracy, a constant load (300 N) is applied in the initial cooling stage until the temperature decreases to the transition temperature. After the cooling stage, the PMMA specimen is demolded from the insert without perceptible adhesion, as shown in Fig. 6(c).

4. Results and discussion

4.1. Fresnel micro-lens array characterization

To characterize the surface geometries and micro-topographies of the diamond turned surface and replicated sample surface, a non-contact white-light interferometer (Talysurf CCI 1000, Taylor Hobson, UK), a laser-probe 2D surface profilometer (NH-3SPs, Mitaka Kohki Co. Ltd., JP) and an optical microscope (OLS4100, Olympus Co. Ltd., JP) under proper magnifications are employed. Fig. 7(a) and (c) illustrate the micrograph of the diamond turned surface and the corresponding cross-section profile along the dotted line, respectively. From the results, the achieved sharp edges on concentric circles without any signs of collisions or scratches indicate the feasibility of the proposed diamond turning method. In addition, these lenslets in the region share almost the same features with no structure and position distortions, which illuminates that a uniform quality of the array is achieved in the diamond turning. Furthermore, the shapes as well as the height of the cross-section profiles along the cross-hair directions match well with each other, indicating high consistence and form accuracy of the machined surface. The intervals between two successive lenslets are measured, 1.212 mm and 1.215 mm in horizontal and vertical directions, and the average height of the lenslets is about 3.142 μm. The measured values match well with the designed ones as shown in Table 1. A similar measurement is also conducted to obtain the surface characteristics of the molded Fresnel micro-lens array, the replicated micro-lens structures and the corresponding profiles along the cross-hair directions shown in Fig. 7(b) and (d). The form accuracy and finished surface quality exhibit similar characteristics as those of the diamond turned mold insert.

Irregular tool vibrations can dramatically change the micro-topography of the machined surface and lead to poor surface roughness. To further analyze the surface integrity of the mold insert and replicated sample, arbitrary lenslets on the mold insert and replicated sample from Fig. 7(a) and (b) are extracted and illustrated in Fig. 8(a) and (b). The 3D structures with a scan area of 900 μm × 900 μm are captured for analyzing surface roughness and form accuracy, as shown in Fig. 8(c) and (d). Three selected zones are abstracted from the mold insert and the replicated sample, respectively. The surface micro-topographies are obtained by removing the geometry form of the lenslets. Correspondingly, the achieved surface roughness values for both the mold insert and replicated sample over three different regions are comparable. For the mold insert, the S_a surface roughness values of the selected areas from the center to the edge are 21.241 nm, 25.110 nm and 23.115 nm, while for the replicated sample, the S_a surface roughness values of the selected areas are 25.203 nm, 26.015 nm and 23.204 nm. Obviously, the surface micro-topography on mold insert is predominated by the periodic residual tool marks in the feed direction. In the cutting direction, the slight fluctuations may correspond to undesired relative vibrations between the diamond tool and the mold insert, indicating that the proposed method effectively restrains tool vibration and enhances the finished surface uniformity. The surface micro-topography on replicated sample presents similar micro features as the mold insert. However, the mold surface achieves a slightly lower surface roughness than the replicated sample, which should be ascribed to two possible reasons. First, deteriorated surface quality of replicated sample might occur at molding temperature due to possible residual water in the molding material, changes of the crystalline structure, or chemical

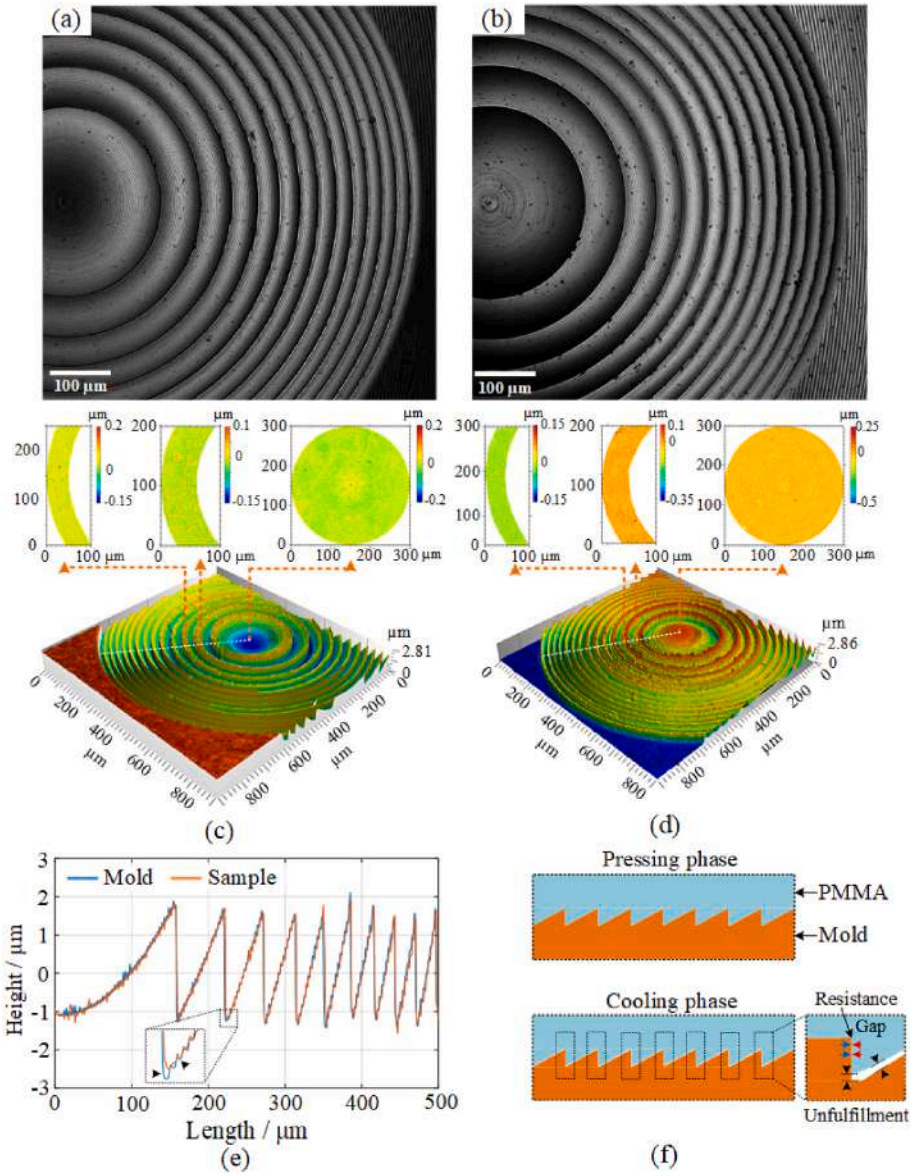

Fig. 8. Microscope diagrams of the (a) mold insert and (b) replicated sample, the 3D structures of the (c) mold insert and (d) replicated sample, (e) the corresponding 2D cross-section profiles along the dashed lines of mold insert and replicated sample, and (f) contraction comparison between the mold insert and replicated sample.

reaction [28], which might result in surface defects after molding process, such as micro bubbles and dents. Second, the residual periodic tool marks on the mold insert exacerbate the differences, since the nano/micro-level surface defects on mold insert lead to insufficient preform-to-mold contact time for inducing deformation on nanoscale, which has been observed and confirmed in previous researches [29].

The cross-section profiles of the mold insert and replicated sample are plotted in Fig. 8(e). By comparing the obtained profiles, the micro-lens structures on the mold insert have been successfully transferred to the PMMA substrate with a slight rounding of the tip. The height difference is less than 0.03 μm between the mold insert and the replicated sample. The difference might be due to the coefficient of thermal expansion (CTE) of the mold insert and the PMMA. In this study, the mold insert material, 6061 Aluminum alloy, have relatively smaller CTE (CTE ≈ 23.2 (units of 10^{-6})) than that of PMMA substrate (CTE ≈ 73, a mean CTE value from ambient temperature to transition temperature). Thus, in the cooling stage, the molded sample contracts more than the mold insert, as shown in Fig. 8(f), which leads to filling defects in the molding process [30,31]. Due to the resistance of the structures of the Fresnel lenslets, the shrinkage of the molded sample along the radius direction in the cooling stage is not remarkable.

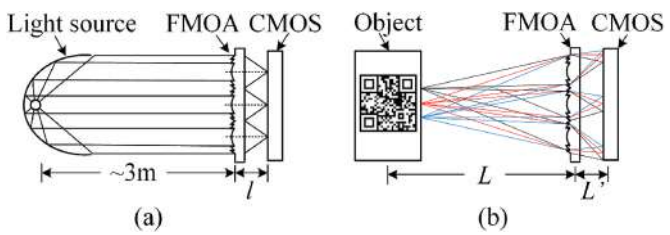

Fig. 9. Schematic diagrams of the optical apparatus for (a) focal point evaluation and (b) imaging testing. FMOA refers to the molded Fresnel micro-lens array.

4.2. Optical performance testing

To evaluate the focusing function and the imaging performance of the molded Fresnel micro-lens array, two groups of optical tests are conducted. The experimental arrangement for focal point evaluation is

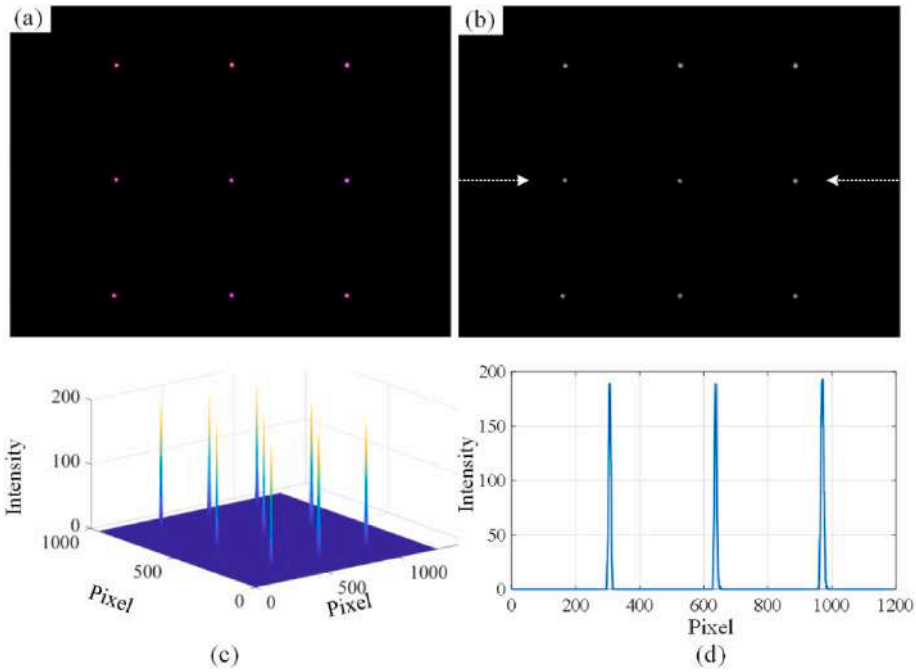

Fig. 10. (a) Measured raw image of the focal spots, focal spot light intensity distribution in (b) 2D and (c) 3D, and (d) focal spot intensity of the selected lenslets.

illustrated in Fig. 9(a). A beam of parallel white light, which is collimated by a parabolic reflector, is projected to the molded Fresnel micro-lens array, and the resulting image is captured by a commercial board-level CMOS detector (1280 × 960 pixels). In addition, for further evaluating the imaging performance of the molded Fresnel micro-lens array, two imaging tests are conducted to demonstrate the optical performance and practicality of the system, including imaging results with a polychromatic object and a monochromatic object. Fig. 9(b) shows the apparatus for the imaging tests. The imaging apparatus consists of an object (screen), the molded Fresnel micro-lens array and the CMOS detector. The screen is a 5.5-inch Retina IPS LCD with 1080 × 1920 pixels. The molded Fresnel micro-lens array is mounted on a 2D micro positioning stage. The distance and angle between the screen and the CMOS detector can be precisely adjusted.

Fig. 10(a) shows the obtained raw image of the focal spot pattern for the 3 × 3 molded Fresnel micro-lens array. The focal points of the Fresnel micro-lens array are uniformly distributed with similar illumination. The spatial intervals are consistent with the distances in the optical design. To further quantify the uniformity of focal point intensity, the original raw image is transferred into light intensity image, as shown in Fig. 10(b) and (c). From the results, the intensity of the focal points agrees well with each other, which proves the uniformity of the molded Fresnel micro-lens array. Meanwhile, the intensity pattern of the selected lenslets, as shown in Fig. 10(d), shows that more than 95% of energy is distributed in the first diffraction order, demonstrating the good focusing performance of the Fresnel lenslets.

Fig. 9(b) shows the imaging principle for the micro-lens array and the corresponding magnification ratio. According to the paraxial imaging law, the object distance L_o and image distance L_i, should follow the equations as follows [32],

$$\frac{1}{L_o}+\frac{1}{L_i}=\frac{1}{f} \tag{8}$$

where f is the focal length of the lens. The magnification ratio is defined as $m = h_i/h_o = L_i/L_m$, while h_i and h_o is the height of image and object, respectively.

The resulting image of a QR code through the 3 × 3 Fresnel micro-lens array is shown in Fig. 11(a). The object distance and image distance are set as 221 mm and 8.3 mm, respectively. Thus, the magnification ratio is 0.037, indicating a reduced image after the imaging system. The obtained image consists of 9 unit-images. Based on the size of each lenslet and the magnification ratio, the effective imaging region for each unit-image is 1.18 mm × 1.18 mm, which covers 325 × 325 pixels. The captured image presents good agreement with the original image, which collects most of the details. However, due to the objects involving polychromatic light, the focal length for each wavelength is not coincident. The iridescent colors occur on the edge of the images. In the other imaging test, a monochromatic object is utilized for imaging, which shows clear edge for the image except the cross-talk images among the neighboring lenslet, as shown in Fig. 11(b).

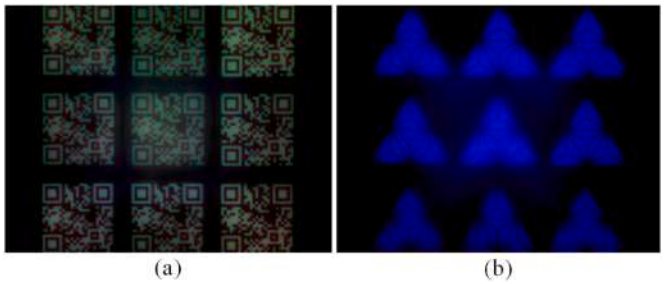

Fig. 11. Photographs of the Fresnel micro-lens array imaging tests using (a) polychromatic object and (b) monochromatic object.

5. Conclusions

In this study, a novel manufacturing approach, involving off-spindle-axis diamond turning and precision glass molding, is first introduced into Fresnel micro-lens array fabrication. The off-spindle-axis toolpath is generated by synchronizing three linear motions and a rotatory motion under servo control. The proposed method is verified experimentally by demonstrating a 3 × 3 Fresnel micro-lens array on a mold insert. The measurement results indicate that the Fresnel micro-lens array mold insert presents high form accuracy and surface integrity. Furthermore, the mold insert is employed in precision glass molding, and the micro-

lens structures are successfully replicated from the mold insert to the PMMA substrate with homogeneous quality. As a demonstration, the molded Fresnel micro-lens array is assembled into an imaging system to capture objects with complex details. The result indicates that the proposed fabrication method overcomes the current difficulties on off-spindle-axis discontinuous profile fabrication, which is particularly suitable for producing mold inserts for large-scale replication of Fresnel micro-lens arrays and other micro-optics array with discontinuous features.

Declaration of competing interest

The authors declare that they have no known competing financial interests or personal relationships that could have appeared to influence the work reported in this paper.

Acknowledgements

Lin Zhang is an International Research Fellow of the Japan Society for the Promotion of Science (JSPS). This study has been financially supported by Grant-in-Aid for JSPS Fellows (Grant No. P20368).

References

[1] Sonneveld PJ, Swinkels GLAM, Tuijl BAJV, Janssen HJJ, Campen J, Bot GPA. Performance of a concentrated photovoltaic energy system with static linear Fresnel lenses. Sol Energy 2011;85(3):432–42.
[2] Kuang Z, Liu D, Perrie W, Edwardson S, Sharp M, Fearon E, Dearden G, Watkins K. Fast parallel diffractive multi-beam femtosecond laser surface micro-structuring. Appl Surf Sci 2009;255(13):6582–8.
[3] Katz B, Rosen J, Kelner R, Brooker G. Enhanced resolution and throughput of Fresnel incoherent correlation holography (FINCH) using dual diffractive lenses on a spatial light modulator (SLM). Opt Express 2012;20(8):9109–21.
[4] Brinksmeier E, Schönemann L. Generation of discontinuous microstructures by diamond micro chiseling. CIRP Ann - Manuf Technol 2014;63(1):49–52.
[5] Jasinevicius RG, Duduch JG, Cirino GA, Pizani PS. Diamond turning of small Fresnel lens array in single crystal InSb. J Micromech Microeng 2013;23:55025.
[6] Chen F, Liu H, Yang Q, Wang X, Hou C, Bian H, Liang W, Si J, Hou X. Maskless fabrication of concave microlens arrays on silica glasses by a femtosecond-laser-enhanced local wet etching method. Opt Express 2010;18(19):20334–43.
[7] Luo S, Chang T, Tsai H. Fabrication of diffractive microlens array by femtosecond laser-assisted etching process. Microelectron Eng 2012;98:448–52.
[8] Deng C, Kim H, Ki H. Fabrication of a compound infrared microlens array with ultrashort focal length using femtosecond laser-assisted wet etching and dual-beam pulsed laser deposition. Opt Express 2019;27(20):28679–91.
[9] Sun R, Li Y, Li L. Rapid method for fabricating polymeric biconvex parabolic lenslets. Opt Lett 2014;39(18):5391–4.
[10] Wang L, Sun R, Vasile T, Chang Y, Li L. High-throughput optical sensing immunoassays on smartphone. Anal Chem 2016;88(16):8302–8.
[11] Yi AY, Li L. Design and fabrication of a microlens array by use of a slow tool servo. Opt Lett 2005;30(13):1707–9.
[12] Yan J, Zhang Z, Kuriyagawa T, Gonda H. Fabricating micro-structured surface by using single-crystalline diamond end mill. Int J Adv Manuf Technol 2010;51:957–64.
[13] Zhu Z, To S, Zhang S. Large-scale fabrication of micro-lens array by novel end-fly-cutting-servo diamond machining. Opt Express 2015;23(16):20593–604.
[14] Chen J, Cheng J, Zhang D, Chen S. Precision UV imprinting system for parallel fabrication of large-area micro-lens arrays on non-planar surfaces. Precis Eng 2016;44:70–4.
[15] Chen C, Huang C, Cheng Y, Hsu W. Ultra-precision diamond milling of aspheric microlens array. Proc. SPIE 2013;8769. 87693Q.
[16] McCall BP, Tkaczyk TS. Fabrication of plastic microlens array for array microscopy by three-dimensional diamond micromilling. Opt Eng 2010;49(10):103401.
[17] Zhang L, Zhou W, Naples NJ, Yi AY. Fabrication of an infrared Shack–Hartmann sensor by combining high-speed single-point diamond milling and precision compression molding processes. Appl Opt 2018;57(13):3598–605.
[18] Sun Z, To S, Zhang G, Zhang S. Flexible fabrication of micro-optics arrays with high-aspect-ratio by an offset-tool-servo diamond machining system. Opt Express 2019;27(7):9631–46.
[19] Zhu Z, To S. Adaptive tool servo diamond turning for enhancing machining efficiency and surface quality of freeform optics. Opt Express 2015;23(16):20234–48.
[20] He Y, Zhou T, Dong X, Liu P, Zhao W, Wang X, Hu Y, Yan J. Generation of high-saturation two-level iridescent structures by vibration-assisted fly cutting. Mater Des 2020;193:108839.
[21] Neo DWK, Kumar AS, Rahman M. An automated Guilloche machining technique for the fabrication of polygonal Fresnel lens array. Precis Eng 2015;41:55–62.
[22] Zhu Z, To S, Tong Z, Zhuang Z, Jiang X. Modulated diamond cutting for the generation of complicated micro/nanofluidic channels. Precis Eng 2019;56:136–42.
[23] To S, Zhu Z, Wang H. Virtual spindle based tool servo diamond turning of discontinuously structured microoptics arrays. CIRP Ann - Manuf Technol 2016;65(1):475–8.
[24] Zhang L, Zhou W, Yi AY. Rapid localized heating of graphene coating on a silicon mold by induction for precision molding of polymer optics. Opt Lett 2017;42(7):1369–72.
[25] Zhang L, Yi AY. Manufacturing of a microlens array mold by a two-step method combining microindentation and precision polishing. Appl Opt 2020;59(23):6945–52.
[26] Yan G, Zhang Y, You K, Li Z, Yuan Y, Fang F. Off-spindle-axis spiral grinding of aspheric microlens array mold inserts. Opt Express 2019;27(8):10873–89.
[27] Yan J, Maekawa K, Tamaki J, Kuriyagawa T. Micro grooving on single-crystal germanium for infrared Fresnel lenses. J Micromech Microeng 2005;15:1925.
[28] Georgiadis K. The failure mechanisms of coated precision glass molding tools. Apprimus Wissenschaftsverlag; 2015.
[29] Zhang Y, Liang R, Spires OJ, Yin S, Yi A, Milster TD. Precision glass molding of diffractive optical elements with high surface quality. Opt Lett 2020;45(23):64386441.
[30] Zhang L, Zhou L, Zhou W, Zhang S, Yi AY. Design, fabrication and testing of a compact large-field-of-view infrared compound eye imaging system by precision glass molding. Precis Eng 2020;66:87–98.
[31] Manaf ARA, Sugiyama T, Yan J. Design and fabrication of Si-HDPE hybrid Fresnel lenses for infrared imaging systems. Opt Express 2017;25(2):1202–20.
[32] Yang T, Liu Y, Mu Q, Zhu M, Pu D, Chen L, Huang W. Compact compound-eye imaging module based on the phase diffractive microlens array for biometric fingerprint capturing. Opt Express 2019;27(5):7513–22.